

Electronic structure of BaIrO_3 : A first principle study using local spin-density approximations

Kalobaran Maiti

Department of Condensed Matter Physics and Material Sciences,
Tata Institute of Fundamental Research, Homi Bhabha Road, Colaba, Mumbai - 400 005, INDIA
(Dated: June 24, 2018)

We investigate the electronic structure of BaIrO_3 , an interesting compound exhibiting charge density wave transition in its insulating phase and ferromagnetic transition at the same temperature, using full potential linearized augmented plane wave method within the local spin density approximations. The ferromagnetic ground state could exactly be described in these calculations and the calculated spin magnetic moment is found to be small as observed in the magnetic measurements. Interestingly, no signature of exchange splitting is observed in the density of states corresponding to Ir 5d and/or any other electronic states. The small spin moment appears essentially due to unequal population of the up- and down-spin Ir 5d bands. Comparison of the valence band density of states with the experimental spectral functions suggests that a rigid shift of the Fermi level towards higher energies in the calculated density of states provides a good description of the experimental spectra. This indicates that the intrinsic oxygen non-stoichiometry leads to electron doping in the system and plays the primary role in determining the electronic structure rather than the electron correlation effects as often observed in other systems. The calculated results for Ba 5p core levels show that the Madelung potential of one of the three non-equivalent Ba atoms is different from that of other two as predicted in the recent experiments.

PACS numbers: 71.20.Lp, 71.15.Ap, 75.25.+z, 71.45.Lr

I. INTRODUCTION

The compound, BaIrO_3 has drawn significant attention in the recent time due to the observation of charge density wave (CDW) transition despite insulating transport observed above and below the CDW transition temperature ($T_c \approx 185$ K).¹ Interestingly, it also exhibits a ferromagnetic transition at the same temperature (185 K) where CDW ground state sets in. The saturation magnetic moment in the ferromagnetic phase, however, is found to be very small ($\sim 0.03 \mu_B$) compared to that expected from the t_{2g}^5 electronic configuration corresponding to Ir^{4+} .

The crystal structure of BaIrO_3 is monoclinic (space group B2/m; unique axis c). In this structure, IrO_6 octahedra form Ir_3O_{12} trimers by face sharing as shown in Fig. 1. The Ir_3O_{12} trimers are inter-linked by corner-sharing to form columns parallel to a -axis. The axis of the connecting trimers are marginally tilted ($\sim 12^\circ$) as shown in the figure.² This leads to the monoclinic structure with the crystallographic angle, $\gamma = 103.27^\circ$. This typical structure makes it a quasi-one dimensional system as has clearly been manifested in the anisotropic transport, magnetic and optical properties.¹ The structure becomes more complex due to the twisting and buckling of the trimers resulting in the multiplicity of Ir-O and Ba-O bond distances, thereby creating 4 types of Ir and 3 types of Ba sites.^{3,4} Different non-equivalent Ir atoms are represented by Ir1, Ir2, Ir3 and Ir4 in the figure. Interestingly, each trimer consists of two non-equivalent Ir atoms. For example, if Ir2 forms the central octahedron of a trimer, it is connected by face sharing to the other two octahedra formed by Ir1. Similarly, the neighboring Ir_3O_{12} trimer

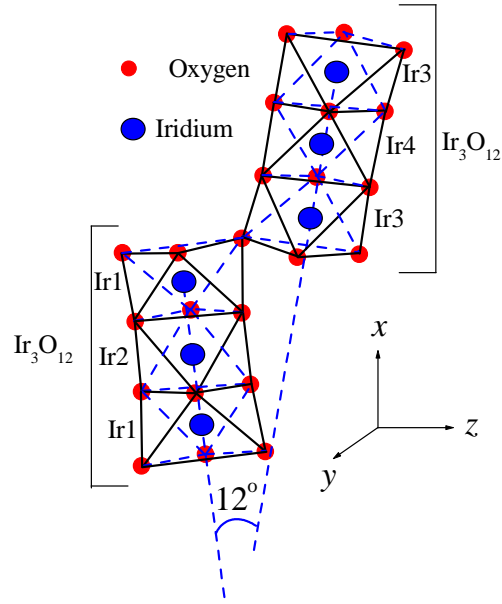


FIG. 1: (color online) Schematic diagram of the Ir_3O_{12} trimers in the monoclinic structure of BaIrO_3 (space group B2/m). The trimers are connected by corner sharing and their long axis are tilted by 12° .

is formed by Ir3 and Ir4, where Ir4 forms the central octahedron and Ir3 forms the other two octahedra. Thus, the inter-trimer link is established along a direction via (Ir1)-O-(Ir3) connectivity.

Despite very short intra-trimer Ir-Ir distances compared to Ir-metal and Ir-O-Ir angle close to 180° for inter-

trimer connections, BaIrO_3 exhibits insulating transport behavior. In addition, there are multiple metal-insulator (MI) transitions within the CDW ground state. While the occurrence of CDW transitions in the insulating phase is surprising, a recent high-resolution photoemission study⁵ reveals the signature of finite density of states at the Fermi level, ϵ_F , at room temperature and it was shown that the CDW ground state evolves by opening a soft gap at ϵ_F across CDW transition temperature. Interestingly, the intensity at ϵ_F in the photoemission spectra at room temperature ($T > T_C$) is significantly small consistent with the observation of very small electronic specific heat coefficient¹ ($\sim 1 \text{ mJ/mole.K}^2$). In contrast, previous theoretical study using extended Hückel tight-binding electronic band structure calculations⁶ exhibits large intensity at ϵ_F as expected for a t_{2g}^5 electronic configuration corresponding to Ir^{4+} . In addition, the analysis of the core level spectra in the photoemission measurements⁵ predicts the existence of two different kinds of Ba sites at room temperature, which become similar before the onset of CDW ground state. All these anomalies^{1,2,3,4,5,6,7,8} in the transport, magnetic and spectroscopic data reveal that BaIrO_3 is truly an exotic material.

Since, the $5d$ orbitals in $5d$ transition metal oxides are highly extended compared to that in $3d$ or $4d$ systems, it is expected that the electron correlation strength will be significantly weak and that the *ab initio* approaches will be successful to describe the electronic properties in this system. In this study, we therefore, investigate the electronic structure of BaIrO_3 using *state-of-the-art* *ab initio* approaches. The calculations for various magnetic configurations suggest that the ground state of BaIrO_3 is ferromagnetic exhibiting small magnetic moments consistent with the experimental observations.¹ The analysis of the valence band density of states in comparison with the experimental photoemission results⁵ suggests that the small intensity at ϵ_F in the photoemission spectra and the insulating transport behavior are presumably related to the pinning of ϵ_F at the upper edge of t_{2g} band due to the intrinsic non-stoichiometry of the samples³ and these edge states are localized due to disorder/crystallographic distortions.^{9,10} The calculations for the Ba $4p$ core levels exhibit signature of two non-equivalent Ba sites with respect to the Madelung potential at the Ba sites in the crystal structure at room temperature.

II. THEORETICAL METHODS

The electronic band structure calculations were carried out using full potential linearized augmented plane wave (FPLAPW) method (Wien2k software¹¹) within the local spin density approximations (LSDA). The crystal structure considered for these calculations has $\text{B}2/\text{m}$ space group with the c -axis as the unique axis. The lattice parameters ($a = 10.005 \text{ \AA}$, $b = 15.174 \text{ \AA}$, $c = 5.571 \text{ \AA}$, $\alpha = \beta = 90^\circ$ and $\gamma = 103.27^\circ$) and the atomic positions used for

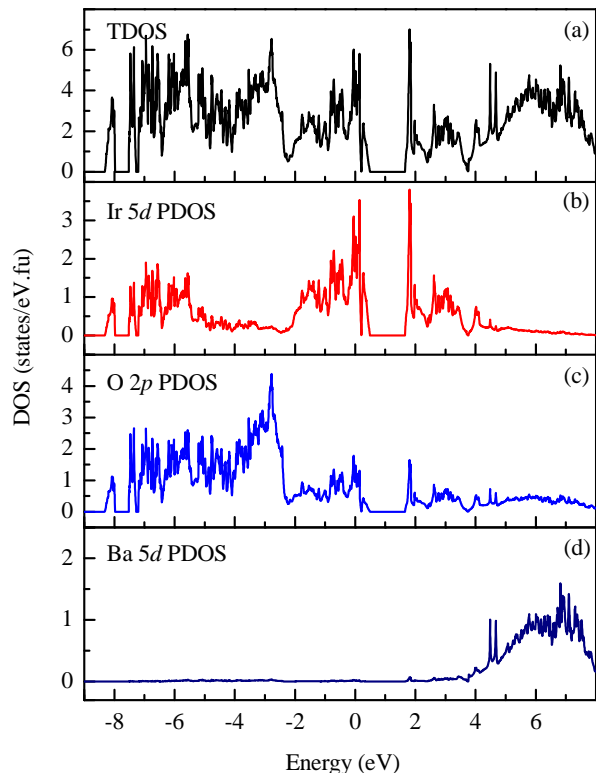


FIG. 2: (color online) Calculated (a) TDOS, (b) Ir $5d$ PDOS, (c) O $2p$ PDOS and (d) Ba $5d$ PDOS for the non-magnetic ground state. The large intensity at the Fermi level suggests a metallic ground state in contrast to the experimental observations. The states at the Fermi level have primarily Ir $5d$ character with O $2p$ states appearing below -2.3 eV.

all the calculations correspond to the room temperature structure reported for well characterized polycrystalline and single crystalline samples in References [1,3]. It is to note here that most of these studies for the crystal structure analysis report the space group as $\text{C}2/\text{m}$ with b axis as the unique axis, which has been transformed to $\text{B}2/\text{m}$ space group by coordinate transformations ($a'b'c' \leftrightarrow acb$) in order to satisfy the requirement of the Wien2k software. The muffin-tin radii (R_{MT}) for Ba, Ir and O were set to 1.217 \AA , 1.111 \AA and 0.847 \AA , respectively. The convergence for different calculations were achieved considering $512 k$ points within the Brillouin zone. The error bar for the energy convergence was set to $< 1 \text{ meV}$.

III. RESULTS AND DISCUSSIONS

In Fig. 2, we show the density of states calculated for the non-magnetic ground state using the lattice parameters corresponding to room temperature structure as mentioned in the previous section. The total density of states (TDOS), Ir $5d$ partial density of states (PDOS), O $2p$ PDOS and Ba $5d$ PDOS are plotted in Fig. 2(a), 2(b), 2(c) and 2(d), respectively. Ba $5d$ electronic states con-

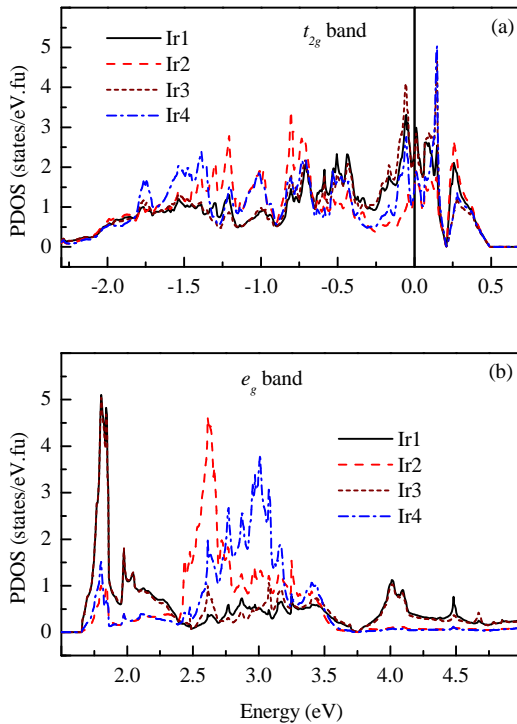


FIG. 3: (color online) Ir 5d band with (a) t_{2g} symmetry and (b) e_g symmetry for all the 4 non-equivalent Ir atoms in the structure. The assignment of Ir atoms are made as shown in Fig. 1.

tribute in the energy range 4 eV above the Fermi level as shown in Fig. 2(d) with almost no contribution at lower energies. O 2p contribution in the Ba 5d dominated energy region is very little, which is expected for the 5d energy level in this heavy alkaline earth atom compared to the cases observed for lighter alkaline earth atoms such as Sr in Sr-compounds or Ca in Ca-compounds having unoccupied 4d and 3d levels, respectively.¹² This suggests that the role of Ba-O covalency in the electronic/crystal structure is not significant in this system.

There are three groups of features observed in TDOS in the occupied part of the electronic structure shown below ϵ_F ($= 0$ eV). The energy range between -5.5 eV to -2.3 eV is primarily dominated by the O 2p PDOS with negligible contributions from Ir 5d PDOS. This suggests that the electronic states in this energy range are not bonded with the Ir 5d states and are known as non-bonding O 2p states. In the energies below -5.5 eV ($-5.5 \text{ eV} > \epsilon > -8.5 \text{ eV}$), O 2p states have the largest intensity with finite contributions from Ir 5d electronic states. Thus, these features can be assigned as bonding bands having primarily O 2p character. The anti-bonding bands having t_{2g} symmetry appears in the energy range -2.5 eV to +0.5 eV (total width ~ 3 eV). The e_g band appears above the Fermi level with a minimum excitation gap of about 1.2 eV from the upper edge of t_{2g} band. The DOS in these regions are essentially contributed by the Ir 5d electronic states with minimal contributions from O 2p states. Thus, the electronic states at and around

ϵ_F have primarily Ir 5d character, which naturally determines the transport, magnetic and other thermodynamic properties. Interestingly, DOS at ϵ_F is found to be significantly large as also observed before⁶ suggesting highly metallic behavior of the system in contrast to the insulating transport, small specific heat coefficient observed¹ and the high-resolution photoemission results recently published.⁵

In order to investigate the contribution from various non-equivalent Ir sites separately, we plot the t_{2g} and e_g band in Fig. 3(a) and 3(b), respectively. The total t_{2g} bandwidth for each of the Ir atoms is found to be close to 3 eV spanning the same energy region. The PDOS corresponding to Ir2 and Ir4 are almost uniformly distributed over the whole energy range. However, Ir1 and Ir3 exhibit largest intensity close to the Fermi level suggesting largest contribution to the conduction electrons. Such a scenario is expected since inter Ir_3O_{12} trimer connectivity is established via (Ir1)-O-(Ir3) superexchange interaction as shown in Fig. 1 and has largest extended character. Ir2 and Ir4 provide intra-trimer connectivity via $d-d$ interactions with Ir1 and Ir3, respectively. Thus, there is a relative shift between the center of gravity of Ir1, Ir3 contributions and Ir2, Ir4 contributions. The features in the energy range $\epsilon < -0.75$ eV has largest contribution from Ir2 and Ir4 sites and for $\epsilon > -0.75$ eV, the intensity arises primarily from Ir1 and Ir3 contributions.

The effective width of the e_g bands is significantly narrower in this system as shown in Fig. 3(b). While Ir2 and Ir4 are primarily contributing in the energies 2.5 eV - 3.5 eV above ϵ_F , the Ir1 and Ir3 contributions appear below 2.5 eV. Interestingly, Ir1 and Ir3 are found to be very similar in both the energy regions, and Ir2 and Ir4 have similar DOS distributions.

Since the axis of any of the IrO_6 octahedra are not aligned along any of the crystal axis as shown in Fig. 1, the t_{2g} bands will have contributions from all the d -orbital states (d_{xy} , d_{yz} , d_{xz} , $d_{x^2-y^2}$ and d_{z^2}) defined in the axis system shown in Fig. 1. The projected partial density of states corresponding to these orbital are shown separately for each of the Ir sites in Fig. 4. Interestingly, the primary contribution ($\sim 35.77\%$) at ϵ_F comes from d_{xz} electronic states located at Ir1 and Ir3 sites. d_{xy} and d_{z^2} at Ir1 and Ir3 sites also exhibit large contributions (14.3% and 16.6% respectively) at ϵ_F . The largest contributions from Ir2 and Ir4, however, arise from d_{xz} (8.4%) and $d_{x^2-y^2}$ (7.6%) electronic states. These numbers clearly manifest that the electronic states containing the quasi-one dimensional axis of the crystal structure (x -axis) have largest contribution at ϵ_F and hence clearly manifests the signature of large anisotropy observed in various bulk properties.¹

We now turn to the understanding of the magnetic behavior of BaIrO_3 . We carried out the spin-polarized calculations using the same crystal structure as in the case of non-magnetic calculations and use local spin density approximations. The magnetic moment has been defined by the difference in occupancy of the majority (up) and

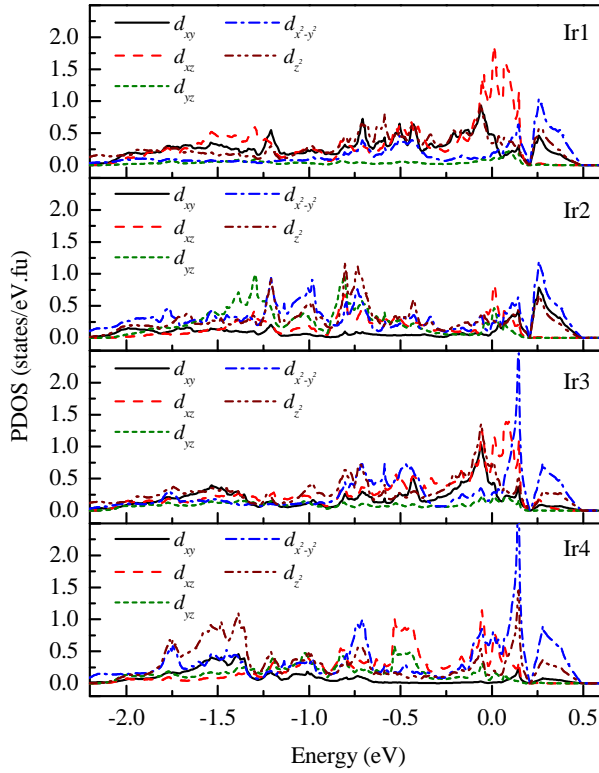


FIG. 4: (color online) PDOS for the t_{2g} band in the non-magnetic ground state having d_{xy} character (solid line), d_{xz} -character (dashed line), d_{yz} -character (short dashed line), $d_{x^2-y^2}$ -character (dot-dashed line) and d_{z^2} -character (dot-dot-dashed line) are shown separately for four non-equivalent Ir atoms.

minority (down) spin states. Spin-orbit interaction was not considered in these calculations. Interestingly, the calculations for various magnetic configurations reveal that the ferromagnetic ground state is 3.25 meV lower than (error bar used for convergence is < 1 meV) the total energy found for the non-magnetic ground state. This energy difference is about 20% of $k_B T_C$ ($T_C = 185$ K). This calculation, thus, once again establish that LSDA approximations are quite accurate in capturing the magnetic ground state of various transition metal oxides as has also been observed in $3d$ transition metal oxides¹³ despite the fact that the electron correlation effects are underestimated in these calculations. The total spin magnetic moment is found to be about $1.34 \times 10^{-3} \mu_B$. This is significantly small compared to that expected for t_{2g}^5 electronic configuration for Ir^{4+} . Such a small value of the spin moment appears presumably due to the highly extended nature of the $5d$ orbitals leading to large kinetic energy of the associated electrons. The calculated spin moment is consistent with the experimental observation of small saturation magnetic moment ($\sim 0.03 \mu_B$) in the magnetic measurements of single crystalline BaIrO_3 ; this moment could be measured only after applying a magnetization field as high as 20 T.¹ No magnetic contribution is found from the Ba-related bands, as all these

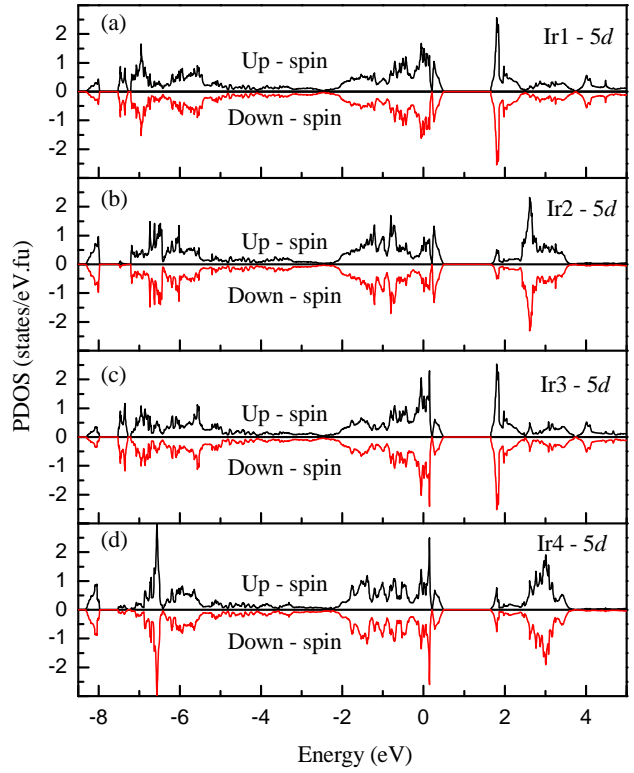


FIG. 5: (color online) Ir 5d PDOS corresponding to ferromagnetic ground state. Up- and down-spin contributions are shown by positive and negative y-axis, respectively. None of the cases show signature of exchange splitting.

bands are either completely occupied and appear much below ϵ_F or completely unoccupied appearing far above ϵ_F . The contribution from O $2p$ states is of the order of $10^{-4} \mu_B$. The primary contribution to the total magnetic moment arises from the spin polarization of Ir 5d partial density of states. Interestingly, all the Ir atoms are found to order ferromagnetically and the magnetic moment at the central Ir site of the Ir_3O_{12} trimer is almost the half of that observed at the other Ir sites.

In Fig. 5, we show the spin-polarized Ir 5d partial density of states for the ferromagnetic ground state, where 5(a), 5(b), 5(c) and 5(d) show the results corresponding to Ir1, Ir2, Ir3 and Ir4 respectively. The down-spin contributions are shown by inverting the y -axis in the same figure with same energy scale for up-spin contributions shown along x -axis. No signature of exchange splitting is observed at any of the Ir sites. The up- and down-spin DOS reveal almost identical structures in all the cases. In order to investigate the origin of the spin moment, we show the total Ir 5d PDOS for both up- and down-spin states in Fig. 6(a) and the difference between up- and down-spin contributions in Fig. 6(b). It is clear that the observed magnetic moment appears due to small asymmetry of the up- and down-spin density of states as a function of energy. Thus, the occupancy of the up- and down-spin contributions is different leading to a small

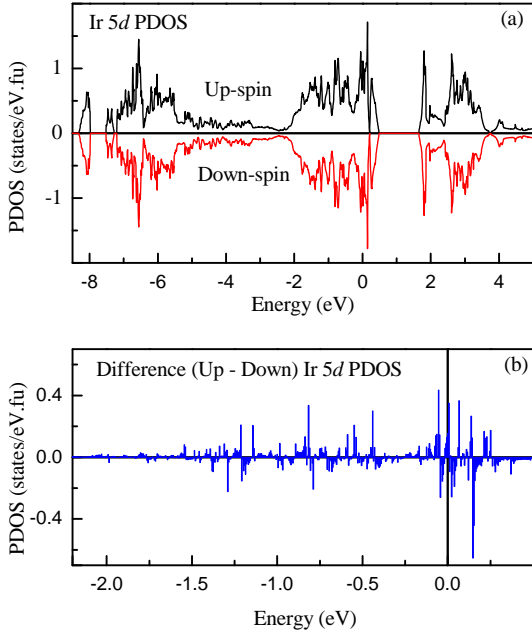


FIG. 6: (color online) Total Ir 5d PDOS corresponding to ferromagnetic ground state. The difference between up- and down-spin PDOS are shown in (b). The spin moment appears due to unequal occupancy of the up- and down-spin bands as shown in the figure.

spin-moment.

Now, we compare the calculated results with the experimental photoemission spectra published recently for BaIrO₃.⁵ In Fig. 7(a), we show the Ir 5d band obtained from He II spectra⁵ and overlap with the calculated t_{2g} band of Ir 5d PDOS. While the calculated results exhibit large intensity at the Fermi level suggesting highly metallic behavior of the system, the experimental Ir 5d feature at room temperature exhibit only very small intensity. The total width of the occupied part in the calculated PDOS is also substantially smaller compared to the Ir 5d signal in the experimental spectra. Such observations of significant reduction of spectral weight at the Fermi level and the population of the higher binding energy region often attributed to the underestimation of electron-electron Coulomb repulsion effect in the *ab initio* approaches. However, such a strong correlation effect in these highly extended 5d electrons is unexpected.

It is to note here that the difference between experimental bulk spectral functions and the *ab initio* results could well be explained in the 4d transition metal oxides¹⁴ using perturbative approach to introduce the correlation effect in the self energy of the system. The effective correlation strength, U/W (U = electron-electron Coulomb repulsion strength, W = bandwidth) was found to be small ($U/W \sim 0.2$) in these systems. We thus calculate the spectral function for BaIrO₃ in the same way, using the second order perturbation method employed by Treglia *et al.*¹⁵ In this method, the spectral function can

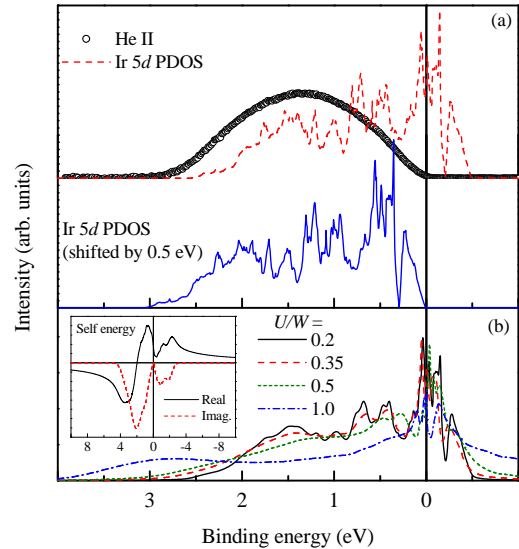


FIG. 7: (color online) (a) The t_{2g} band (dashed line) obtained from *ab initio* calculations is compared with the experimental Ir 5d band (circles) delineated from the He II spectrum. The experimental results are adopted from Ref. [5]. The calculated DOS is significantly different from the experimental ones. The calculated DOS shifted by 0.5 eV towards higher binding energies (solid line) reveal better description of the experimental spectrum. (b) Spectral functions obtained by introducing electron correlation effects into the self energy by second order perturbative approach using *ab initio* results. The change in U/W leads to a spectral weight transfer toward higher binding energies. The inset shows the real (solid line) and imaginary (dashed line) part of the self energy.

be expressed as,

$$f(\epsilon) = -\frac{1}{\pi} \text{Im} \sum_k G_k(\epsilon)$$

where, $G_k(\epsilon)$ is the retarded Green's function representing the many electron system and is given by

$$G_k(\epsilon) = \frac{1}{(\epsilon - \Sigma_k(\epsilon) - \epsilon_k)}$$

where, $\Sigma_k(\epsilon)$ is the self energy of the system. For small U , $\Sigma_k(\epsilon)$ can be calculated using perturbation approach upto the second order term^{15,16} within the local approximations. We have used Ir t_{2g} PDOS shown in Fig. 7(a) as the band DOS for these calculations. The calculated spectral functions for different U/W are shown in Fig. 7(b) and the calculated self energy is shown in the inset of the same figure. The increase in U/W leads to a significant spectral weight transfer to higher energies. The new features appearing at higher binding energies due to such spectral weight transfer is known as incoherent feature and represent the electronic states essentially localized due to such correlation effect. The feature at the Fermi level represent the delocalized states and is known as coherent feature. The total weight of the coherent feature diminishes gradually with the increase in U/W .

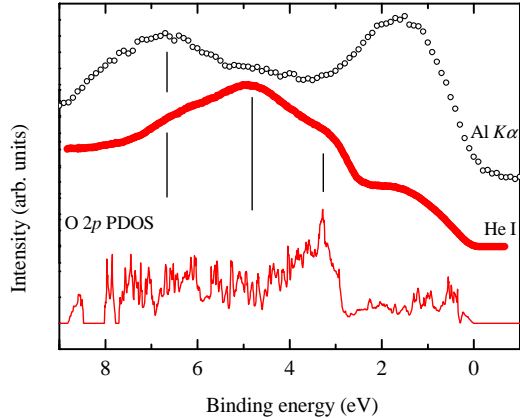


FIG. 8: (color online) Experimental He I (solid circles) and Al $K\alpha$ spectra (open circles) adopted from Ref. [5] are compared with the calculated O $2p$ PDOS (solid line) shifted by 0.5 eV towards higher binding energies.

However, the intensity at the Fermi level remains almost the same for U/W as large as 1.0. The spectral function obtained in this process could not generate the spectral lineshape observed in the experimental spectrum for any value of U/W . This suggests that this procedure may not be adequate to determine the experimental results.

Interestingly, a rigid shift of the calculated t_{2g} band by 0.5 eV towards higher binding energies provide a significantly good description of the experimental spectrum. The width and spectral distribution in the shifted spectral function shown in Fig. 7(a) is remarkably similar to that observed in the Ir $5d$ band in the He II spectrum. In order to investigate this further we compare the O $2p$ PDOS with the experimental spectra as it is well known that the *ab initio* calculations are quite successful to provide a good description of the O $2p$ band even in $3d$ transition metal oxides.¹³ We show the experimental Al $K\alpha$ and He I spectra in Fig. 8 adopted from Ref. [5]. The changes in these experimental spectra in the energy range between 3 eV to 9 eV binding energies concomitant to the change in relative photoemission cross section¹⁷ of the O $2p$ and Ir $5d$ electronic states suggest that the features in 3-6 eV binding energies appear primarily due to the excitations of O $2p$ non-bonding states and the intensity at higher binding energies are due to the bonding electronic states having large O $2p$ character. Interestingly, the calculated O $2p$ PDOS shows the intense non-bonding O $2p$ features around 2.3-5.5 eV binding energies with the peak at 2.8 eV binding energy (see Fig. 2), where the dip appears in the He I spectrum. This clearly suggests that it is necessary to shift the O $2p$ PDOS by at least 0.5 eV towards higher binding energies to compare with the experimental spectra. The shifted O $2p$ PDOS shown by solid line in Fig. 8 provide a good description of the experimental results.

Thus, the results in Fig. 7 and Fig. 8 suggest that the Fermi level is shifted to the upper edge of the t_{2g} band presumably due to the electron doping into the system.

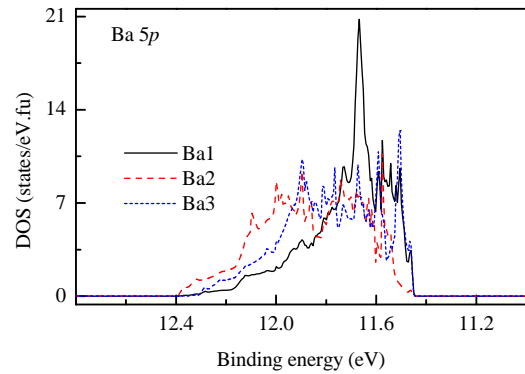


FIG. 9: (color online) Calculated Ba $5p$ DOS corresponding to 3 non-equivalent Ba atoms present in the monoclinic structure. The results show that Ba2 contributions appear at higher binding energies compared to that in other Ba atoms

Such a shift would stabilize the system due to the closeness to the fully filled electronic configuration resulting to lowering in energy. Interestingly, various experimental results indeed indicate that the oxygen content is often found to be less than 3.0,^{3,7} which effectively leads to electron doping into the Ir $5d$ band. In addition, the transport measurements always exhibit insulating temperature dependence.¹ Such a behavior is not unusual since it is natural that the small intensity at the upper edge of the t_{2g} band will be localized due to the disorder and/or crystallographic distortions^{9,10} in this quasi-one dimensional structure leading to an insulating nature. All these observations, thus, clearly indicate that the electron correlation may not be the primary origin for the differences between experimental and theoretical results. The electron doping due to the oxygen non-stoichiometry intrinsic to BaIrO₃ possibly plays the key role in determining the electronic structure and subsequently various physical properties in this system.

We now turn to the question of multiple Ba core level signals in the experimental spectra.⁵ We show the DOS corresponding to Ba $5p$ core levels in Fig. 9. There are three non-equivalent Ba sites in the structure with respect to the Ba-O bond length and the symmetries. It is clear that the DOS corresponding to Ba1 and Ba2 appear in the same energy range. While the width of the DOS corresponding to Ba2 $5p$ states is similar to those corresponding to Ba1 and Ba3, the peak position appear at higher binding energies. The energy difference between these spectral features is about 0.25 eV. This observation clearly suggests that the Madelung potential at all the Ba sites are not same and is consistent with the experimental observation of two non-equivalent features corresponding to each Ba core level photoemissions. Such relative shift of the DOS corresponding to different non-equivalent Ir atoms is not observed in these calculations (e.g. see Fig. 3 for the t_{2g} bands corresponding to 4 non-equivalent Ir sites).

IV. CONCLUSIONS

In summary, we investigate the detailed electronic structure of BaIrO_3 in this study using full potential linearized augmented plane wave method within the local spin density approximations. The calculations for various magnetic configurations reveal lowest energy for the ferromagnetic ground state and is consistent with the experimental observations. The ferromagnetic ground state energy calculated using room temperature crystal structure is found to be 3.25 meV lower than the non-magnetic ground state. No exchange splitting is observed in any of the electronic states involved in forming the valence band. The small magnetic moment appears due to unequal population of the different Ir 5d spin density of

states.

Comparison with the photoemission spectra suggests that electron- electron Coulomb repulsion may not be the key factor in determining the electronic structure as expected for the highly extended nature of the 5d electronic states. The discrepancy between the experimental spectra and the calculated results appears to arise primarily from the intrinsic non-stoichiometry of BaIrO_3 leading to electron doping into the t_{2g} band. The calculations for Ba 5p core levels exhibit the signature of multiple non-equivalent Ba sites in the room temperature structure as observed experimentally. Thus, these results provide a significant advance towards understanding the electronic properties of the exotic compound, BaIrO_3 .

¹ G. Cao, J.E. Crow, R.P. Guertin, P.F. Henning, C.C. Homes, M. Strongin, D.N. Basov, and E. Lochner, Solid State Commun. **113**, 657 (2000).

² R. Lindsay, W. Strange, B.L. Chamberland, and R O Moyer, Jr., Solid State Commun. **86**, 759 (1993).

³ A.V. Powell and P.D. Battle, J. Alloys and Compounds **232**, 147 (1996).

⁴ T. Siegrist and B.L. Chamberland, J. Less-Common Met. **170**, 93 (1991).

⁵ K. Maiti, R.S. Singh, V.R.R. Medicherla, S. Rayaprol, and E.V. Sampathkumaran, Phys. Rev. Lett. **95**, 016404 (2005).

⁶ M.-H. Whangbo and H.-J. Koo, Solid State Commun. **118**, 491 (2001).

⁷ B.L. Chamberland, J. Less-Common Met. **171**, 377 (1991).

⁸ G. Cao, X. N. Lin, S. Chikara, V. Durairaj, and E. Elhami, Phys. Rev. B **69**, 174418 (2004); A. Ohnishi, M. Sasaki, Y. Kuroda, M. Sato, Y. Isobe, and G. Cao, Physica B **329**, 930 (2003).

⁹ N.F. Mott *Metal-Insulator Transitions*, 2nd ed. (Taylor & Francis, London, 1990).

¹⁰ P.W. Anderson, Phys. Rev **109**, 1492 (1958).

¹¹ P. Blaha, K. Schwarz, G.K.H. Madsen, D. Kvasnicka, and J. Luitz, **WIEN2k**, An Augmented Plane Wave + Local Orbitals Program for Calculating Crystal Properties (Karlsheinz Schwarz, Techn. Universität Wien, Austria), 2001. ISBN 3-9501031-1-2.

¹² E. Pavarini, S. Biermann, A. Poteryaev, A. I. Lichtenstein, A. Georges, and O. K. Andersen, Phys. Rev. Lett. **92**, 176403 (2004).

¹³ D. D. Sarma, N. Shanthi, S. R. Barman, N. Hamada, H. Sawada, and K. Terakura, Phys. Rev. Lett. **75**, 1126 (1995).

¹⁴ K. Maiti and R.S. Singh, Phys. Rev. B **71**, 161102(R) (2005).

¹⁵ G. Treglia, F. Ducastelle, and D.G. Spanjaard, J. Physique **41**, 281 (1980); G. Treglia, F. Ducastelle, and D. Spanjaard, Phys. Rev. B **21**, 3729 (1980).

¹⁶ D. D. Sarma, F. U. Hillebrecht, W. Speier, N. Mårtensson, and D. D. Koelling, Phys. Rev. Lett. **57**, 2215 (1986).

¹⁷ J.J. Yeh and I. Lindau, *At. Data and Nucl. Data Tables* **32**, 1 (1985).